JOURNAL OF APPLIED ELECTROCHEMISTRY 8 (1978) 121–134

The potentiodynamic behaviour of copper in NaOH solutions

A. M. CASTRO LUNA DE MEDINA, S. L. MARCHIANO, A. J. ARVÍA

Instituto de Investigaciones Fisicoquímicas Teóricas y Aplicadas (INIFTA), División Electroquímica, Sucursal 4, Casilla de Correo 16, 1900 La Plata, Argentina

Received 25 May 1977

The potentiodynamic behaviour of Cu in different NaOH solutions at 25° C is studied paying particular attention to the anodic formation and cathodic reduction of the Cu(I) and Cu(II) surface species occurring during the electrochemical processes. The potentiodynamic response of the electrochemical interface is strongly dependent on the perturbation conditions and it reveals the complexity of the electrochemical reactions occurring there as well as the inter-relation of the processes taking place at different potentials. A reaction pathway to interpret the corresponding behaviour is advanced.

1. Introduction

Although there are a relatively large number of publications dealing with the anodic oxidation of copper in alkaline solutions, the knowledge of the process is still rather limited. The conclusions of the different authors diverge, particularly with regard to the kinetics and mechanism related to the formation of the passivating layer on the metal [1–17]. The latter when it is galvanostatically formed at 25° C, as deduced from X-ray diffraction [4, 6, 7], consists of $Cu(OH)_2$ at $i \leqslant 0{\cdot}5$ mA cm^{-2}, while CuO is the only product found when $i \geqslant 0{\cdot}8$ mA cm^{-2}. At intermediate current densities a $Cu(OH)_2$ and CuO mixture is produced. The two anodic reaction products are related to the complex *E/I* profile resulting under potentiodynamic conditions [16] in the Cu/Cu(II) potential range.

Three different reaction mechanisms have been advanced to interpret the copper passivation process; (a) a precipitation–dissolution mechanism [9]; (b) a nucleation and growth mechanism [14–15] and (c) a combined mechanism [17]. The latter, which is postulated to correlate the voltammetric and scanning electron microscopy results, implies a growth mechanism for the lower $Cu(OH)_2$ layer and a nucleation and growth from the solution mechanism for the upper $Cu(OH)_2$ layer. The distribution of both layers depends upon the potential applied at the interface and on the perturbation conditions. The thermodynamically stable CuO phase would be slowly formed from $Cu(OH)_2$.

Most of the mechanistic conclusions were drawn from experimental data restricted to the Cu/Cu(II) potential range and within a relatively narrow alkaline concentration. The voltammetric studies evidenced complex *E/I* traces for Cu in alkaline solutions covering a potential range which extended from the O_2-evolution region to the H_2-evolution region and the voltammogram shape depended strongly among other factors on the limits of the potential sweep. Therefore, this encouraged the investigation of the potentiodynamic behaviour of copper in alkaline solutions covering a wide range of potential perturbation conditions and alkaline solution concentration. The study also presents the possible contribution of solid-phase transformations in the films formed during copper passivation, which corresponds in the *E/I* trace to a kind of film-ageing process.

2. Experimental

A conventional three-compartment electrolysis cell was employed. Different disc working electrodes axially mounted on Teflon rods were employed. Two of them were made of copper (3·14 mm^2 and 12·6 mm^2, respectively) and another one of platinum (7·5 mm^2). Both kinds of electrodes were used either as such or copper-plated, depending on the purpose of the experiments.

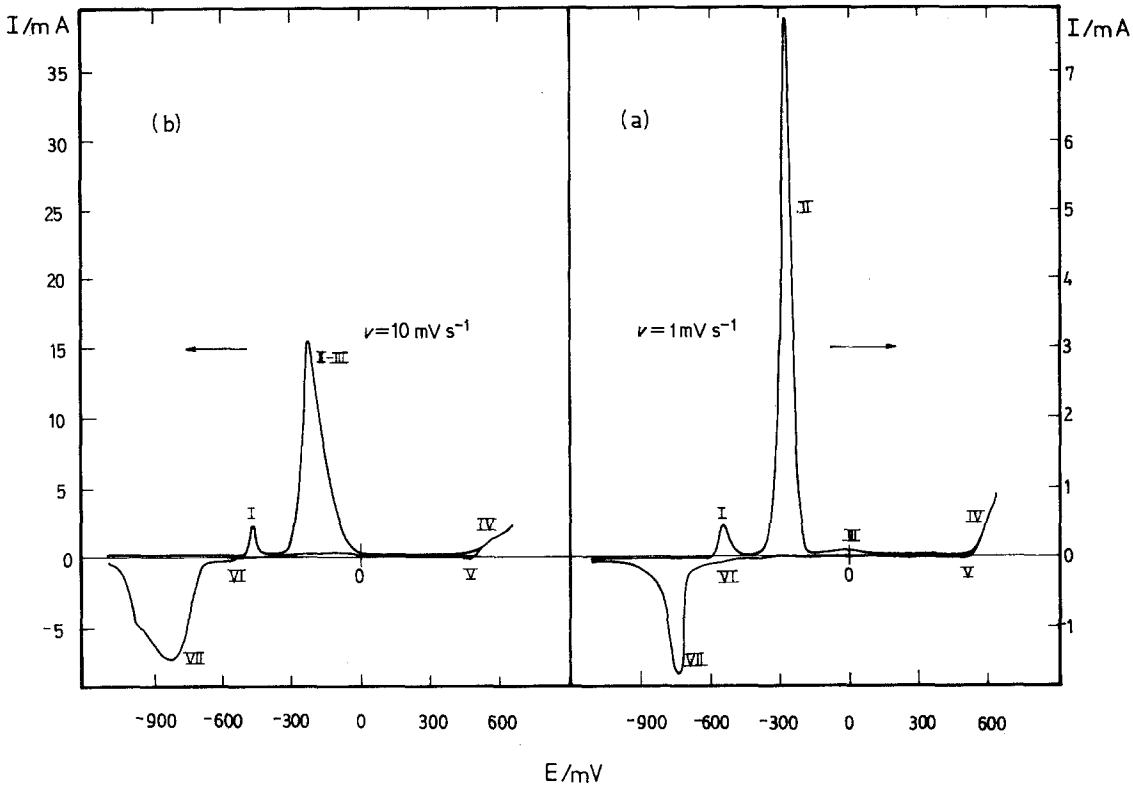

Fig. 1. Potentiodynamic E/I displays run with single triangular potential scans; 2 M NaOH, 26° C, electrode area 0·126 cm^2: (a) 1 mV s^{-1}; (b) 10 mV s^{-1}.

A saturated calomel electrode was used as reference. The counterelectrode was a Pt sheet (4·3 cm^2). The following electrolytic solutions, prepared from AR chemicals and triply distilled water, were used: (a) x M NaOH ($10^{-2} \leqslant x \leqslant 2$ M); (b) x M NaOH + y M $NaClO_4$ ($10^{-2} \leqslant x \leqslant 2$ M; $y = 3 \times 10^{-1}$ M); (c) 2 M NaOH + $Cu(OH)_2$ (sat). Solutions previously deoxygenated were employed under N_2-saturation. The circuitry of the present work is the same already employed in previous work [18].

Different electrode treatments were tested, such as; (a) mechanical polishing with ultra-fine alumina and degreasing; (b) copper-plating at different current densities from a $CuSO_4/H_2SO_4$ solution, at room temperature; (c) chemical etching with different aggressive solutions [19] at room temperature; (d) electropolishing following a conventional procedure [20]. The first electrode surface treatment yielded the best reproducible E/I traces and was selected for the runs shown in the present work.

3. Results

3.1. *Copper electrodes*

The E/I characteristics of mechanically polished electrodes in NaOH solutions depend: (a) on the rate of potential perturbation; (b) on the number of potential scans when repetitive triangular potential scans are used; (c) on the anodic ($E_{\lambda,a}$) and cathodic ($E_{\lambda,c}$) limits covered during the potential excursions; and (d) on the electrolyte concentration.

The voltammetric runs in 2 M NaOH started from −1·11 V up to 0·695 V, at 0·001 V s^{-1} (Fig. 1a) show good defined voltammograms with three sharp current peaks at $c.$ −0·540 (peak I), at −0·226 V (peak II) and at $c.$ 0 V (peak III). Preceding the O_2-discharge, a small shoulder at $c.$ 0·600 V (peak IV) is recorded. During the cathodic scan a small cathodic current in the vicinity of 0·585 V(VI) and a well-defined cathodic current peak at −0·735 V (peak VII) are observed.

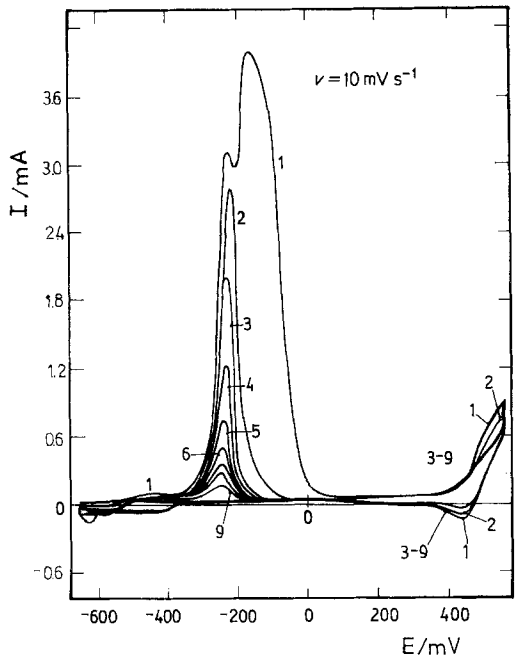

Fig. 2. Potentiodynamic *E/I* displays run with repetitive triangular potential scans; 2 M NaOH, electrode area 0·126 cm², 26° C.

The same experiment at 0·010 V s^{-1} (Fig. 1b) shows, in principle, the same features, but the peaks II and III are now closer together approaching a single current peak profile. The cathodic current peak VII becomes more complex and the complementary characteristics of current peaks IV and V become more noticeable. As the scanning rate (ν) increases the trace corresponding to current peaks II and III becomes broader but the anodic charge decreases.

Under repetitive potential scans, in 2 M NaOH, the *E/I* repetitive traces depend both on n, the potential scan number (Fig. 2) and on $E_{\lambda,c}$. When $E_{\lambda,c} = -0{\cdot}650$ V, at any ν, the heights of current peaks I and II progressively decrease as n increases. The charge (Q) involved in current peaks IV and V also decreases, although slightly, as n increases. When $E_{\lambda,c} = -1{\cdot}0$ V, the height and charge of current peak I decreases as n increases but no appreciable change is observed in current peak VI. In the potential range of current peaks II and III, at any ν, there is a slight tendency to a charge increase during the first potential sweeps, the shape of the *E/I* contour remaining practically unaltered. Otherwise, current peak VII shifts towards more cathodic potentials as n increases without further

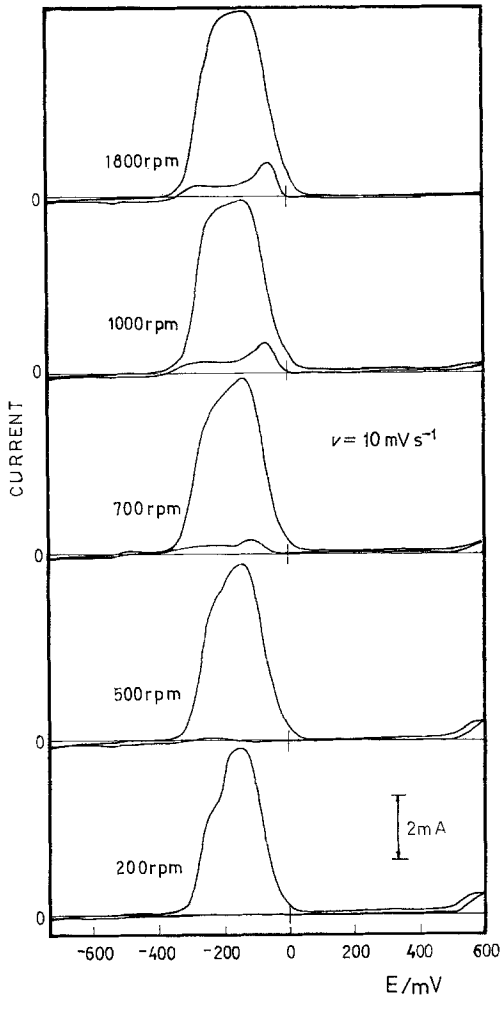

Fig. 3. Stirring effect on the potentiodynamic *E/I* profiles; 2 M NaOH, electrode area 0·126 cm², 26° C.

change of the corresponding contour. This effect is better observed at low ν (0·01 V s^{-1}) since at large ν the cathodic shift of the peak makes its area less clearly defined.

The influence of the rotation speed, at 0·01 V s^{-1} (Fig. 3), is to slightly increase the total anodic charge for any of the NaOH concentrations employed. The cathodic scan exhibits a small anodic current peak at the potential of the current peak III and an anodic current plateau which covers a potential range coinciding with the width of current peak II. This effect becomes less noticeable when the NaOH concentration decreases as the concentration of soluble anion copper species also decreases, and when the potential sweep rate increases. The amount of cathodic charge com-

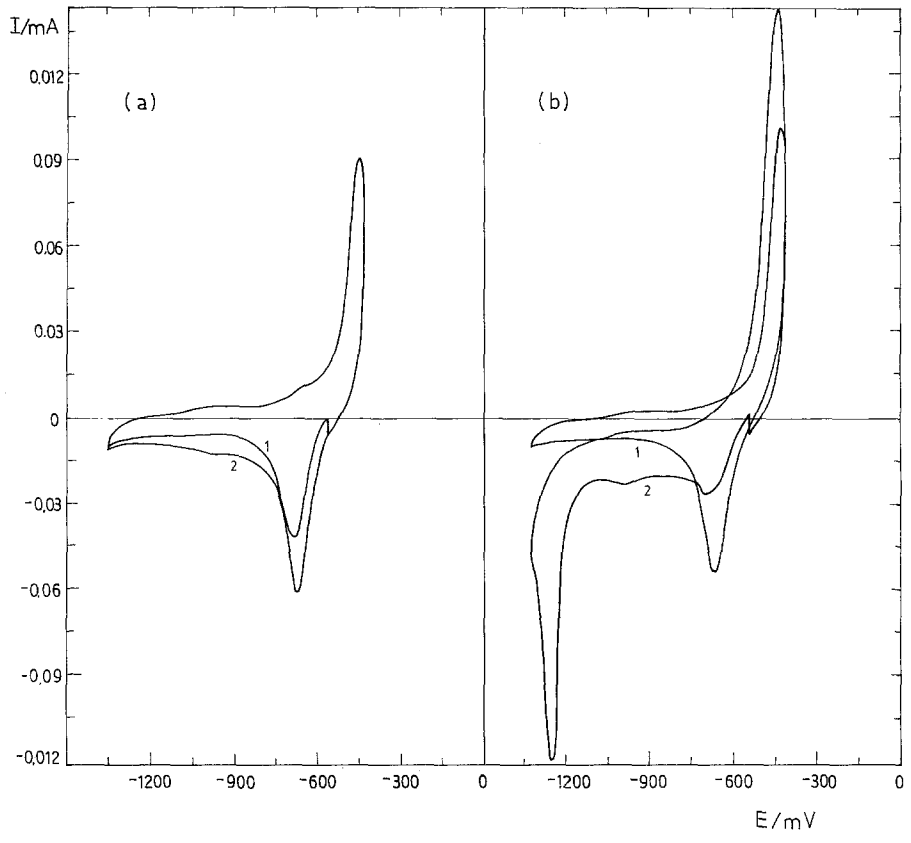

Fig. 4. Potentiodynamic E/I profiles at 100 mV s^{-1} including different waiting times, τ, during the cathodic scan; 2 M NaOH, 26° C, electrode area 0·0314 cm^2: (a) $\tau = 50$ s; (b) $\tau = 200$ s. Curve 1 corresponds to $\tau = 0$.

prised in the reverse scan also increases slightly with the rotation speed. The largest effect is observed when the limits of the potential scan correspond to those of the anodic current peaks II and III.

The E/I profiles run between −1·35 V and −0·435 V, at 0·1 V s^{-1}, involving an interruption of the cathodic potential scan at a potential where the net current is close to zero (Fig. 4), shows a definite change of the continuous cathodic E/I profile. Thus, when the interruption time is short (less than 100 s), although the total cathodic charge remains practically constant, the height of current peak VI decreases and its potential becomes slightly more cathodic; also the cathodic current in the remaining potential range increases. When the interruption time is larger than 100 s, two new cathodic current peaks are seen at $c.$ −0·690 V and $c.$ −1·26 V and, under these circumstances, Q_c becomes larger than Q_a.

The first potential sweep run with 1 M NaOH at 0·1 V s^{-1} covering from −0·8 to 0·35 V (Fig. 5) shows current peak I at −0·43 V and a relatively wide current peak with a maximum at $c.$ −0·175 V, involving at least two current peaks (II and III). Under the same perturbation conditions in 1 M

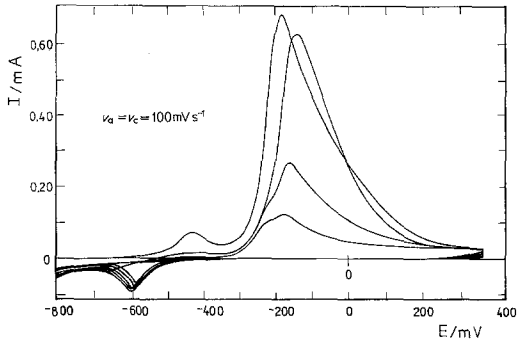

Fig. 5. Potentiodynamic E/I displays at 100 mV s^{-1} run with repetitive triangular potential scans. The successive cycles are numbered; 1 M NaOH, electrode area 0·126 cm^2, 24·4° C.

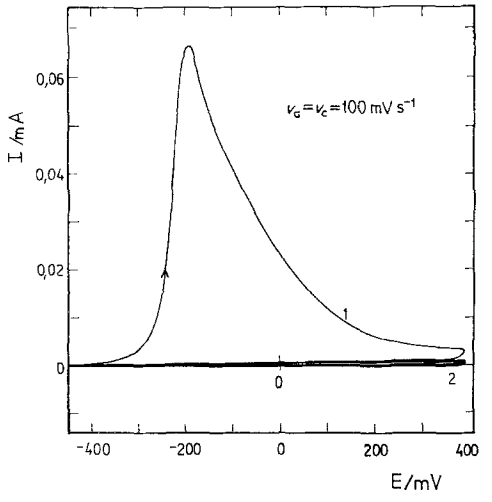

Fig. 6. First and second potentiodynamic E/I profile at 100 mV s^{-1}: passivation effect; 1 M NaOH, electrode area 0·0314 cm^2, 26° C.

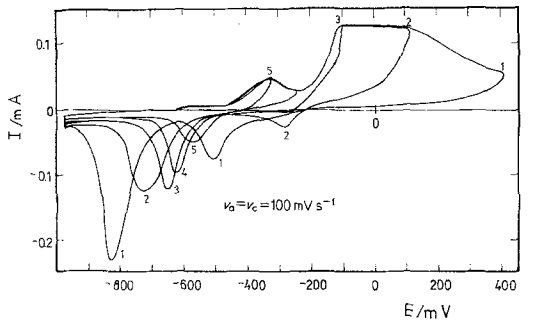

Fig. 7. Influence of $E_{\lambda,a}$ on the potentiodynamic E/I profile at 100 mV s^{-1}; 10^{-1} M NaOH, electrode area 0·0314 cm^2, 25° C.

NaOH the latter is wider than in 2 M NaOH. Peak I disappears in the following potential scans and peaks II and III are well-defined during the following potential cycles. Current peak III, unlike in the 2 M NaOH solution, is always seen in the E/I trace. During the cathodic scan from 0·35 V downwards, there is practically no current until the potential is *c.* −0·4 V. The cathodic current peak VI at *c.* −0·600 V becomes more negative during cycling, as in the 2 M solutions.

The E/I contour depends also on the anodic potential limit reached. The E/I traces obtained involve a systematic decrease of $E_{\lambda,a}$ and a constant $E_{\lambda,c}$ with electrodes previously cycled, reproducing the results published earlier by Ambrose, Barradas and Shoesmith [14].

At potential sweeps from −0·4 to 0·4 V the electrode surface is completely passivated just after the first potential excursion. The passive state is maintained during the following potential cycling (Fig. 6).

A series of potential sweeps run with a 0·1 M NaOH solution and an electrode which has attained a stable E/I contour after cycling at 0·1 V s^{-1} covering different $E_{\lambda,a}$ (Fig. 7) show, particularly during the reversal cathodic scan, an E/I contour depending on $E_{\lambda,a}$. The more extended anodic sweep exhibits a small current plateau in the −0·61 V to −0·46 V range followed by a wide current peak at −0·35 V and a third anodic current region between −0·225 V and 0·375 V, involving at least two current peaks located at *c.* −0·120 V and *c.* 0·070 V, respectively.

When $-0{\cdot}170\ \text{V} \leqslant E_{\lambda,a} \leqslant 0{\cdot}4\ \text{V}$ the returning cathodic sweep presents, at a constant potential, an anodic current which is larger as $E_{\lambda,a}$ becomes more cathodic. When $E_{\lambda,a} = 0{\cdot}4$ V two cathodic current peaks are recorded at −0·525 V and at

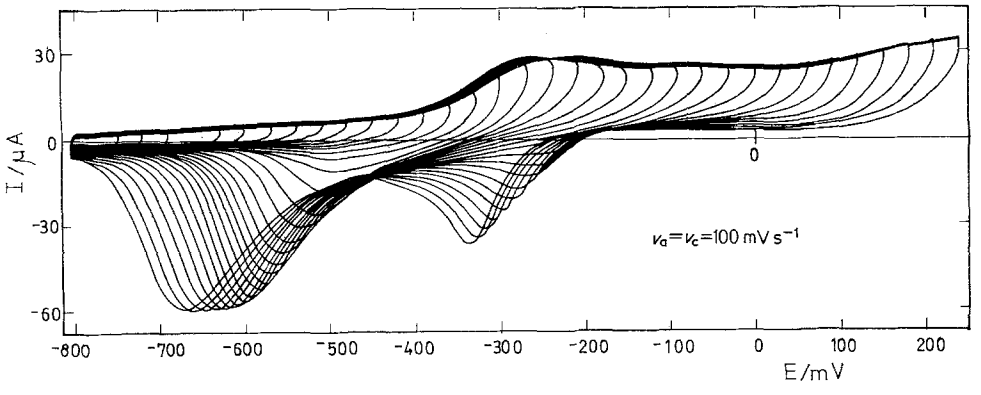

Fig. 8. Influence of $E_{\lambda,a}$ on the potentiodynamic E/I profile at 100 mV s^{-1}; 10^{-2} M NaOH + 3 × 10^{-1} M $NaClO_4$, electrode area 0·0314 cm^2, 26° C.

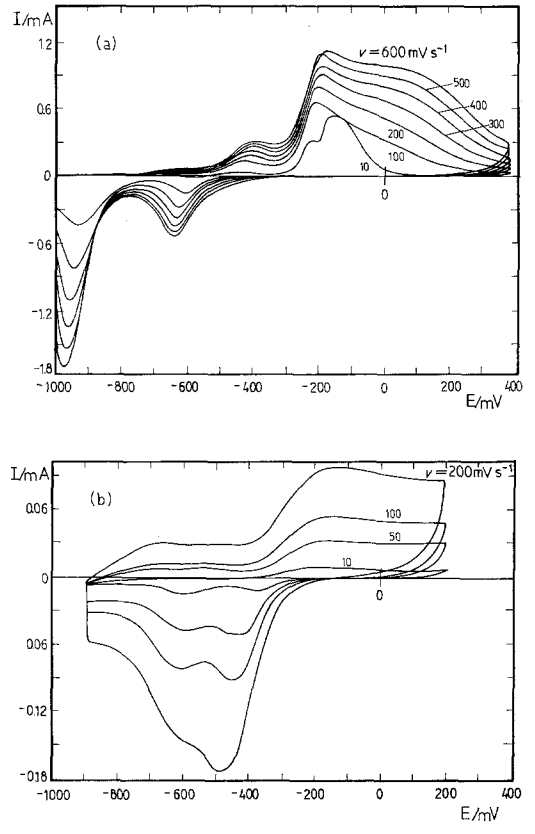

Fig. 9. Influence of ν and NaOH concentration on the potentiodynamic E/I profiles run with single triangular potential sweeps. Electrode area 0·0314 cm², 25° C: (a) 1 M NaOH; (b) 10^{-2} M NaOH + 10^{-1} M $NaClO_4$.

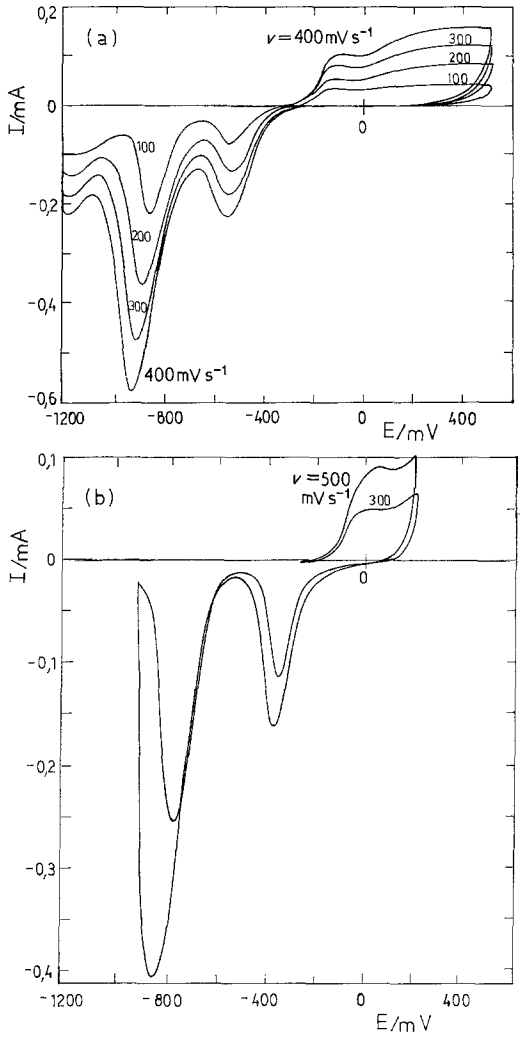

Fig. 10. Potentiodynamic E/I profiles run with single asymmetric triangular potential sweeps at different ν. Electrode area 0·0314 cm², 25° C: (a) 10^{-1} M NaOH; (b) 10^{-2} M NaOH + 10^{-1} M $NaClO_4$.

−0·840 V, respectively, the former being preceded by a small current wave. As $E_{\lambda,a}$ decreases, the two current peak potentials become more anodic, while their current heights decrease. Finally, when $E_{\lambda,a} \leqslant -0{\cdot}130$ V, only one cathodic current peak is observed during the cathodic scan, its potential being −0·575 V when $E_{\lambda,a} = -0{\cdot}330$ V.

A series of E/I profiles run with 10^{-2} M NaOH containing 0·3 M $NaClO_4$ under symmetrical triangular potential perturbations initiated from −0·80 V towards different $E_{\lambda,a}$, involved a single broad and ill-defined anodic current wave from c. −0·370 V upwards with two or even more current peaks. The returning cathodic profiles depend quite strongly on $E_{\lambda,a}$(Fig. 8).

The three anodic current peaks are, in principle, observed at low potential sweep rates for different NaOH concentrations (Fig. 9). In fact, in 2 M NaOH the three anodic current peaks are more clearly distinguished than at lower NaOH concentrations.

Thus, the current peak II grows at the expense of current peak III and when ν_a increases, the width of current peak II increases, overlapping to a large extent the anodic current peak I. The overlapping of the anodic peaks is larger as the NaOH concentration decreases, attaining, for 10^{-1} and 10^{-2} M NaOH, a sort of extended current plateau.

By running the voltammograms with 10^{-1} M and 10^{-2} M NaOH from $E_{\lambda,c} = -0{\cdot}3$ V up to $E_{\lambda,a} = 0{\cdot}5$ V and the following reverse potential excursion to $E_{\lambda,c} = -0{\cdot}12$ V at different ν, the cathodic current peaks show a good definition (Fig. 10). The heights of both peaks are approximately linearly dependent on ν_c and the correspond-

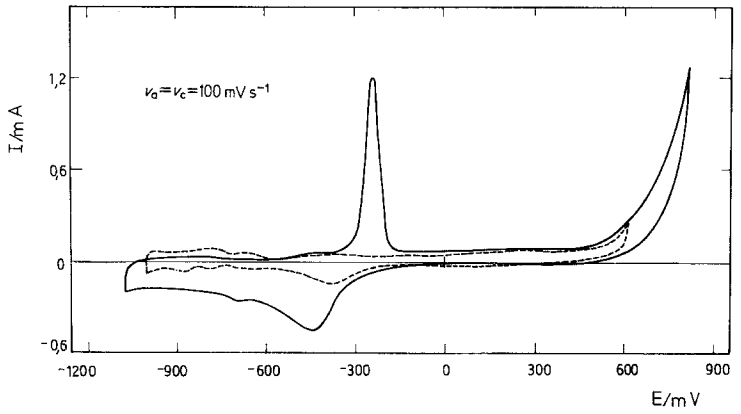

Fig. 11. Potentiodynamic E/I profiles run with single triangular potential sweeps, starting in the cathodic direction at 100 m V s^{-1}. Pt electrode (0·075 cm^2). 2 M NaOH + $Cu(OH)_2$ (sat), 26° C. Dashed line corresponds to a blank without $Cu(OH)_2$.

ing current peak potential becomes more cathodic as the latter increases. These dependences, however, are only of qualitative significance since the cathodic charge decreases quite markedly as ν_c increases.

3.2. *Copper-plated platinum electrodes*

Some anodic E/I profiles were recorded at 0·1 V s^{-1} with a symmetrical triangular potential perturbation and a 2 M NaOH solution saturated with $Cu(OH)_2$ to yield cuprite ions, covering from −1·08 V to +0·82 V (Fig. 11). They are somewhat like those already described with Cu electrodes, particularly, within the −0·6 V to 0·2 V potential range, but for the present system the anodic peak is confined to a narrower potential range.

Current peaks IV and V insinuate in the potential region preceding the oxygen discharge. The reverse cathodic scan shows an appreciable current contribution in the −0·3 V to −0·9 V range. This is probably related to the presence of cuprite ions at a higher concentration than in the previous cases. At the more cathodic potentials the electrodeposition of copper takes place.

The E/I profiles depend upon the limits of the potential excursion and the rate of the potential perturbation. Thus, when $E_{\lambda,a} = 0{\cdot}54$ V and $E_{\lambda,c} = -0{\cdot}96$ V (Fig. 12), the E/I display shows two main anodic current peaks, one at −0·48 V and another quite remarkable one at −0·25 V, and during the cathodic scan two relatively small current peaks at −0·420 V and −0·670 V, respectively. In principle, these E/I displays are independent of $E_{\lambda,a}$ when the latter extends from 0 V to almost 0·54 V, but the current peak at −0·42 V decreases accordingly.

The most reproducible results were obtained by electrodepositing a fixed amount of copper on platinum at a constant cathodic sweep rate ($\nu_c = 0{\cdot}01$ V s^{-1}, $E_{\lambda,c} = -0{\cdot}83$ V and $E_{\lambda,a} = 0$ V) (Fig. 13a) including a constant ageing of the metal film electrodeposited. Then, the influence of ν_a on the anodic E/I profile can be determined. There is

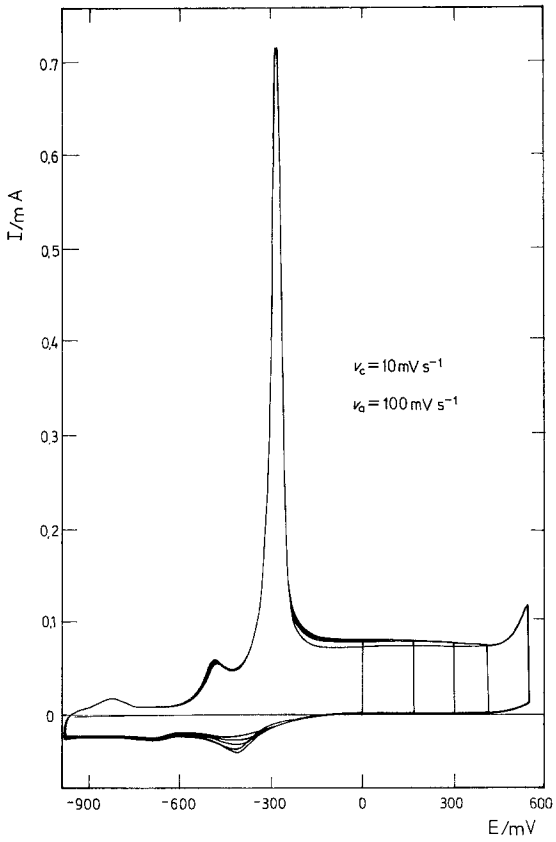

Fig. 12. Potentiodynamic E/I profiles run with single triangular potential sweeps starting from different $E_{\lambda,a}$. Pt electrode (0·075 cm^2), 2 M NaOH + $Cu(OH)_2$ (sat), 26° C.

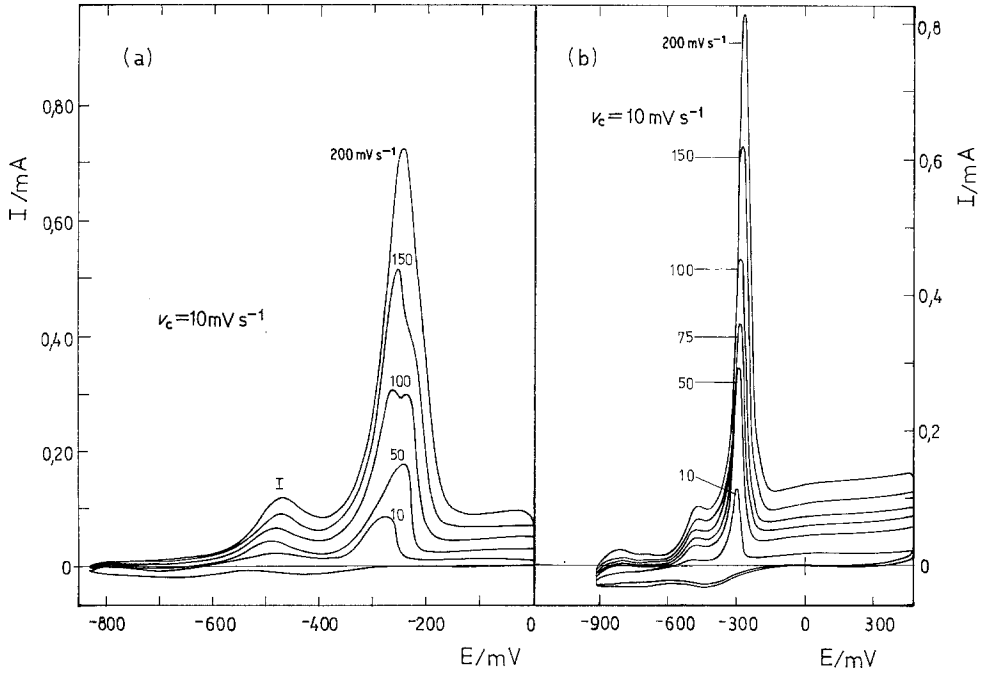

Fig. 13. Effect of v and $E_{\lambda,a}$ on the potentiodynamic profiles. Pt electrode (0·075 cm²), 2 M NaOH + $Cu(OH)_2$(sat), 26° C: (a) $E_{\lambda,a} = 0$ V; (b) $E_{\lambda,a} = 0{\cdot}480$ V.

a broad anodic current peak at $c.\ -0{\cdot}5$ V and another one at $c.\ -0{\cdot}275$ V. When $v_a = 0{\cdot}1\ V\,s^{-1}$, the latter splits into two current peaks, one at

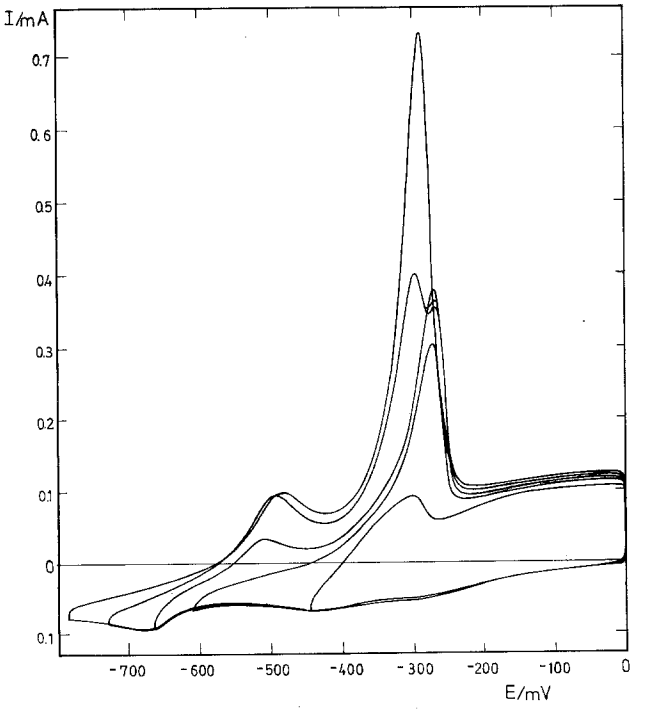

Fig. 14. Influence of $E_{\lambda,c}$ on the potentiodynamic E/I profiles. Pt electrode (0·075 cm²), 2 M NaOH + $Cu(OH)_2$ (sat), 25° C.

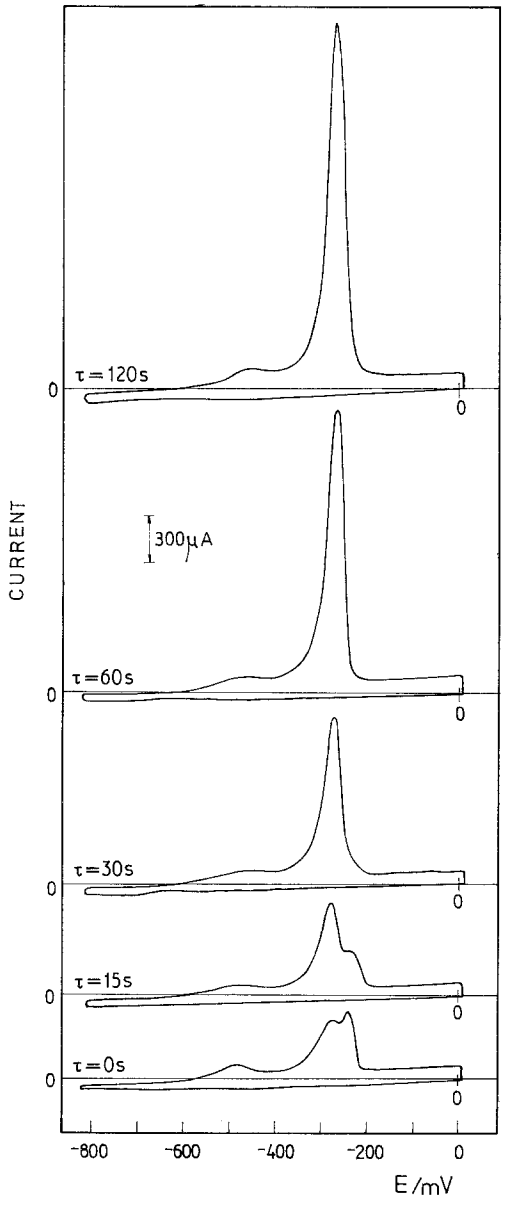

Fig. 15. Potentiodynamic E/I profiles involving different waiting times at $-0{\cdot}8$ V; $\nu_c = 10$ mV s^{-1}; $\nu_a = 50$ mV s^{-1}, Pt electrodes (0·075 cm^2), 2 M NaOH + $Cu(OH)_2$ (sat), 26° C.

$-0{\cdot}235$ V (III) and another at $-0{\cdot}265$ V (II). As ν_a increases the height of current peak II increases faster than that of current peak III. This response, however, depends upon the conditions prevailing during the metal film formation, (ν_c and $E_{\lambda,c}$), (Fig. 13b). On increasing $E_{\lambda,a}$ and $E_{\lambda,c}$ the anodic current peak at c. $-0{\cdot}3$ V prevails as a sharp current peak whose height increases approximately with $\nu_a^{1/2}$. Otherwise, when the amount of electrodeposited copper increases, the anodic charge also increases and the distribution of the current peaks located between $-0{\cdot}2$ V and $-0{\cdot}3$ V changes.

The E/I displays initiated from $E_{\lambda,a} = 0$ V towards cathodic potentials at $\nu_c = 0{\cdot}01$ V s^{-1} and $\nu_a = 0{\cdot}05$ V s^{-1} with increasing $E_{\lambda,c}$ during the successive cycles (Fig. 14) exhibit a systematic change of the E/I contour with $E_{\lambda,c}$. During the anodic scan the anodic current peak I is only observed when $E_{\lambda,c} = -0{\cdot}6$ V. On the other hand the anodic current peak II is related to the occurrence of current peak I while the anodic current peak III is apparently independent of it.

The voltammograns run at $\nu_c = 0{\cdot}01$ V s^{-1} and $\nu_a = 0{\cdot}05$ V s^{-1} and $E_{\lambda,c} = -0{\cdot}8$ V including a variable waiting time, τ, at $E_{\lambda,c}$ (Fig. 15), exhibit the tendency of current peak III to disappear as τ increases. Simultaneously the height of current peak II increases systematically, its potential becoming more anodic. The amount of anodic charge related to current peak I remains practically independent of τ while that related to the current peaks II and III increases with the amount of copper electrodeposited.

After anodizing the copper-plated Pt-electrodes at different potentials the following species are detected by X–ray diffractometry. At $-0{\cdot}9$ V, only the Cu spectrum is observed. At $-0{\cdot}5$ V the main species in Cu_2O and at $-0{\cdot}25$ V CuO prevails. These results also apply to the copper electrodes.

4. Discussion

Different copper-containing species can exist in equilibrium either in solution or at the electrode surface, depending on the solution pH, as seen in the copper/aqueous solution potential/pH diagram [21]. The different equilibria and their corresponding Nernst equations are assembled in Table 1.

A straightforward comparison between the region of potentials involved in the E/I traces and the possible equilibria together with the dependence of the potential of the various current peaks on pH, favours the assignation of current peaks I and VI to the reactions involving the Cu/Cu(I) species, either as Cu^+ or Cu_2O. The potential range of anodic current peaks II and III

Table 1. Equilibria involved at the Cu–NaOH interface

1.	$HCuO_2^- + 3H^+ + e = Cu^+ + 2H_2O$	$E_o = 1{\cdot}733 - 0{\cdot}1773\ pH$
2.	$Cu_2O + 2H^+ + 2e = 2Cu + H_2O$	$E_o = 0{\cdot}471 - 0{\cdot}0591\ pH$
3.	$2HCuO_2^- + 4H^+ + 2e = Cu_2O + 3H_2O$	$E_o = 1{\cdot}783 - 0{\cdot}1182\ pH + 0{\cdot}0591 \log(HCuO_2^-)$
4.	$2CuO_2^{2-} + 6H^+ + 2e = Cu_2O + 3H_2O$	$E_o = 2{\cdot}560 - 0{\cdot}1773\ pH + 0{\cdot}0591 \log(CuO_2^{2-})$
5.	$2CuO + 2H^+ + 2e = Cu_2O + H_2O$	$E_o = 0{\cdot}669 - 0{\cdot}0591\ pH$
6.	$2Cu(OH)_2 + 2H^+ + 2e = Cu_2O + 3H_2O$	$E_o = 0{\cdot}747 - 0{\cdot}0591\ pH$
7.	$CuO + H_2O = HCuO_2^- + H^+$	$\log(HCuO_2^-) = -18{\cdot}83 + pH$
8.	$Cu(OH)_2 = HCuO_2^- + H^+$	$\log(HCuO_2^-) = -17{\cdot}52 + pH$
9.	$HCuO_2^- = CuO_2^{2-} + H^+$	$HCuO_2^-/CuO_2^{2-}\ pH = 13{\cdot}5$

corresponds to the formation of Cu(II) species, either as $Cu(OH)_2$, CuO, $HCuO_2^-$ or CuO_2^{2-} and finally, the potential region just preceding the O_2-evolution is related to the Cu(II)/Cu(III) redox couple (peaks IV and V). This description of the *E/I* traces as far as the possible reactions is concerned, agrees, in principle, with previous interpretations [14, 15].

The *E/I* displays involving the Cu/Cu(I) species exhibit an appreciable separation between the potentials corresponding respectively to the anodic and cathodic current peaks which increases slightly as v increases. This separation increases when $E_{\lambda,a}$ increases, and even more markedly when $E_{\lambda,a}$ exceeds the potential of current peak I. The amount of charge, Q_a, playing a part in the anodic process diminishes quite rapidly when v increases (Table 2). An extrapolation of Q_a at $v \to \infty$ by plotting Q_a v. $1/v$, yields $(Q_a)_{v\to\infty} \approx 1900\ \mu C\ cm^{-2}$ which corresponds to the minimum amount of charge related to the formation of the Cu_2O film on copper. The average film thickness is about 230 nm.

Table 2. Anodic charge of current peak I at different v

v ($mV\ s^{-1}$)	$Q_a \times 10^3$ ($C\ cm^{-2}$)
1	180
10	27
100	5

Experiments covering the $E_{\lambda,c}$ and $E_{\lambda,a}$ limits constrained to the Cu/Cu(I) species, show that the Q_a:Q_c charge ratio within this potential range is close to one. The initial portions of either the anodic or the cathodic *E/I* profiles give Tafel lines. Their slopes, however, increase as v increases. Nevertheless at a constant v, both Tafel lines intercept at a potential which lies close to the equilibrium potential of reaction 2 (Table 1). This agrees with the anodic formation of Cu_2O on the electrode surface as determined by X–ray diffractometry. Unfortunately, no simple relationships between the potential sweep rate and either the current peak height or the current peak potential are established.

The cathodic voltammogram, on the other hand, shows that when the species anodically formed is kept for different times, τ, at the null current potential region immediately after its electroformation, its potentiodynamic electroreduction profile exhibits the current peak shifted towards more cathodic potentials, the potential shift depending on τ. This reveals that besides the proper electrochemical reaction there is also a chemical transformation of the initial film-forming species into another more stable one. Furthermore, the anodic product also dissolves as a Cu(II) species, which is evidenced by the remarkable increase of Q_c when τ is larger than 100 s.

Since the Cu_2O film electroformation *E/I* profile depends on the potential range swept and reveals the occurrence of chemical transformation and dissolution processes, the overall reaction

should involve a series of steps which yield an intermediate OH-containing surface species together with a chemical step yielding the stable Cu_2O, according to the following sequence of reactions

$$(n\mathrm{Cu}) + \mathrm{OH}^- \rightleftharpoons [(n-1)\mathrm{Cu}\,(\mathrm{CuOH})] + \mathrm{e} \quad (1a)$$

$$[(n-1)\mathrm{Cu}\,(\mathrm{CuOH})] + \mathrm{OH}^- \rightleftharpoons [(n-2)\mathrm{Cu}\,2(\mathrm{CuOH})] + \mathrm{e} \quad (1b)$$

$$\vdots \qquad\qquad \vdots$$

$$[(n-m)\mathrm{Cu}\,m(\mathrm{CuOH})] + \mathrm{OH}^- \rightleftharpoons \{[n-(m+1)]\mathrm{Cu}\,(m+1)\,(\mathrm{CuOH})\} + \mathrm{e} \quad (1z)$$

where the brackets indicate the metallic phase covered by either an incompleted or a completed layer of the CuOH-species and where n is the total number of copper atoms available for electrooxidation. The scheme is completed by admitting the possibility of an electrooxidation yielding Cu_2O and H^+ which can be generalized through a series of single charge transfer steps such as

$$[(n-m)\mathrm{Cu}\,m(\mathrm{CuOH})] \rightleftharpoons \{[n-(m+1)]\mathrm{Cu}\,(m-1)(\mathrm{CuOH})(\mathrm{Cu_2O})\} + \mathrm{H}^+ + \mathrm{e} \quad (2a)$$

$$\vdots \qquad\qquad \vdots$$

$$\{[n-m+(y-1)]\mathrm{Cu}[m-(y-1)]\,(\mathrm{CuOH})(y-1)(\mathrm{Cu_2O})\} \rightleftharpoons \{[n-(m-y)]\mathrm{Cu}\,(m-y)(\mathrm{CuOH})\,y(\mathrm{Cu_2O})\} + \mathrm{H}^+ + \mathrm{e} \quad (2z)$$

and, as a possible limiting reaction,

$$\{[n-(m+1)]\mathrm{Cu}\,(m+1)(\mathrm{CuOH})\} \rightleftharpoons \{[n-(m+1)]\mathrm{Cu}[(m+1)/2]\mathrm{Cu_2O}\} + [(m+1)/2]\mathrm{H_2O}. \quad (3)$$

A reaction pathway such as (1–3) becomes very complex when the overall reaction involves a multilayer formation. The formation of Cu(II) species at this stage should proceed through a relatively slow chemical reaction which is promoted either by the proper decrease of pH at the interface or, more likely, by a chemical disproportionation of the various compounds which form the oxidized heterogeneous multilayer film. The ageing-type effect noticed during the film electroreduction is a rather complex process which probably entails an accommodation of O-atoms in the oxide layer into a more stable configuration.

The fact that Q_a increases when v decreases should be related to the occurrence during the film formation of processes such as either the chemical surface transformation or the contribution of the chemical dissolution of the film as suggested by Barradas *et al.* [14, 15] or both acting simultaneously in the same direction. The dissolution involving the chemical formation of Cu(II) whose electroreduction is related to the cathodic current peak at *c.* −0·780 V in Fig. 1, should imply an overall reaction such as

$$\{[n-(m+1)]\mathrm{Cu}\,(m-1)(\mathrm{CuOH})(\mathrm{Cu_2O})\} + \mathrm{OH}^- \rightleftharpoons \{(n-m)\mathrm{Cu}\,(m-1)(\mathrm{CuOH})\} + \mathrm{HCuO_2^-} \quad (4)$$

which corresponds to a disproportionation of the Cu_2O species into a Cu(II) and Cu species, the former dissolving in the alkaline medium as either $HCuO_2^-$ or CuO_2^{2-} according to the solution pH.

The overall reaction yielding mainly Cu_2O species may become controlled by any of the following possible steps: (a) copper diffusion from the bulk metal when the first monolayer is completed; (b) either OH^- diffusion from the solution or H^+ diffusion out of the interface; (c) surface diffusion of any of the oxygen containing species; (d) the rate of the chemical reaction and (e) by nucleation and growth. However, different rate determining steps may act during the dynamic electrochemical formation and electrodissolution of the Cu_2O-containing film depending on the perturbation conditions. Then, it is rather unlikely to obtain any simple quantitative relationship between the perturbation variables and either the current peak height or the peak potential.

The anodic current peak located between 0 V and −0·3 V exhibits complex characteristics. At least two anodic current peaks are distinguished and the total anodic charge involved is larger than that of the preceding anodic current peak corresponding to Cu_2O formation. At the highest NaOH concentration, current peak II increases more rapidly when v_a increases while

at lower ν_a current peak III predominates. One observes also the following characteristics: (a) when $E_{\lambda,a}$ is located within the region of these current peaks, the initial portion of the returning cathodic scan is practically superposed onto the anodic *E/I* trace and exhibits a cathodic current which increases as $E_{\lambda,a}$ decreases; this can be taken as an indication that the product formed only in the potential range of current peak II is electroreduced there. (b) The potential of the cathodic current peaks becomes more negative as $E_{\lambda,a}$ increases. This effect might be related to the different pH at the interface when the cathodic sweep is initiated from a more positive potential since the increase of anodic charge certainly implies a local pH increase; as a matter of fact, this effect is more marked as the NaOH concentration decreases. (c) During the first cycle ($-0{\cdot}650\,V \leqslant E_{\lambda,c} \leqslant 0{\cdot}600$ V) one observes that current peaks II and III appear when Cu_2O was formed previously. This suggests that a direct Cu → Cu(II) electrooxidation is unlikely in the corresponding potential range; on the contrary a Cu electrooxidation through a continuously reforming Cu_2O film may occur. (d) Current peak III involves the passivation of copper, the final reaction product being the stable CuO, as indicated by Shoesmith *et al.* [17]. (e) When the potentiodynamic profile is obtained under stirring, the anodic charge slightly increases and during the returning cathodic scan the corresponding anodic current increases with the rotation speed. This reveals the occurrence of another partial chemical dissolution of the passive film formed, either $Cu(OH)_2$ or CuO, yielding either $HCuO_2^-$ or CuO_2^{2-}, which diffuses away. The composition of the film formed within the potential range of current peaks II and III corresponds to $[xCu(OH)_2 + yCuO]$ where $0 \leqslant x \leqslant 1, 0 \leqslant y \leqslant 1$ and $x + y = 1$, depending on the perturbation conditions [16].

These characteristics indicate that different compounds involving Cu(II) species are continuously formed during the potential sweep covering current peaks II and III. From the potentials where these processes occur (see Table 1) and the influence of pH both in the location of the current peaks and in the distribution of current product, the corresponding overall reaction can be understood in terms of a sequence of steps such as

$$\{[n-(m+1)]\,Cu\,(m+1)(CuOH)\} + OH^- \rightleftharpoons \{[n-(m+1)]\,Cu\,m(CuOH)Cu(OH)_2\} + e \quad (5a)$$

$$\{[n-(m+1)]\,Cu\,m(CuOH)Cu(OH)_2\} + OH^- \rightleftharpoons \{[n-(m+1)]\,Cu\,(m-1)(CuOH)2Cu(OH)_2\} + e. \quad (5b)$$

Simultaneously, copper electrodissolution takes place according to

$$\{[n-(m+1)]\,Cu\,(m-1)(CuOH)\,2Cu(OH)_2\} + OH^- \rightleftharpoons \{[n-(m+2)]\,Cu\,m(CuOH)\,2Cu(OH)_2\} + e \quad (6)$$

and finally when the $Cu(OH)_2$ is formed

$$\{[n-(m'+p')]\,Cu\,m'(CuOH)\,p'Cu(OH)_2\} + m'OH^- \rightleftharpoons \{[n-(m'+p')]\,Cu\,(p'+m')\,Cu(OH)_2\} + m'e. \quad (7)$$

The above reaction sequence implies no specific stoichiometry between various species of hydroxy- and oxy-copper and copper atoms in the lattice since the corresponding coefficients vary over the surface. Moreover, the overall reaction under potentiodynamic conditions comprises a time variation of the surface composition either on the electrode plane or inside the layer.

Current peak II which is mainly related to $Cu(OH)_2$ electroformation involves a charge larger than current peak I, therefore $(m' + p') > (m + 1)/2$. This reaction sequence can also be initiated from the Cu_2O-containing species. The overall reaction is in either case represented by Equation 6 in Table 1.

The porous characteristics of the $Cu(OH)_2$-containing film may in part be due to a contribution of a Cu electrodissolution as Cu(II) which further precipitates on the surface as the hydroxide species. The latter either produces a thickening of the film or dissolves in part as a Cu(II)-containing species.

The $Cu(OH)_2$ surface product formed in Equation 7 reacts at least in part with the alkaline media yielding one of the soluble species CuO_2^{2-} or $HCuO_2^-$ depending on pH, according to

$$\{nCu\,p\,[Cu(OH)_2]\} \rightleftharpoons \{nCu\,(p-q)\,Cu(OH)_2\} + qHCuO_2^- + qH^+ \quad (8a)$$

$$\{n\mathrm{Cu}\ p[\mathrm{Cu(OH)_2}]\} \rightleftharpoons \{n\mathrm{Cu}\ (p-q)\ \mathrm{Cu(OH)_2}\} + q\mathrm{CuO_2^{2-}} + 2q\mathrm{H^+} \quad (8b)$$

The $[Cu(OH)_2 + CuO]$-containing film is electrochemically transformed into a CuO-type film at higher anodic potential than that corresponding to current peak II.

The electrooxidation of the $Cu(OH)_2$-covered Cu gives an H^+ ion and a CuO species, starting from one of the following compounds:

$$\{[n-(m'+p')]\mathrm{Cu}\ (m'+p')\mathrm{Cu(OH)_2}\} \rightleftharpoons \{[n-(m'+p'+1)]\mathrm{Cu}[m'+p'-1)]\ \mathrm{Cu(OH)_2}\ 2\mathrm{CuO}\} + 2\mathrm{H^+} + 2\mathrm{e} \quad (9)$$

until all the $Cu(OH)_2$ surface is transformed into CuO. Then, the total passivation of the metal is achieved.

The formation of the CuO species means that the film acquires a more compact structure, which facilitates the onset of metal passivity.

The reaction pathway, although particularly involved, explains that the surface products obtained in this potential range are a mixture of oxy- and hydroxy-compounds with the prevalence of either one, depending on the anodic potential. The chemical transformation of the $Cu(OH)_2$ species into the CuO one, as suggested by Shoesmith *et al.* [17], is a reaction parallel to the electrochemical process

$$[\mathrm{Copper} + x\mathrm{Cu(OH)_2} + y\mathrm{CuO}] \rightleftharpoons [\mathrm{Copper} + (x+y)\mathrm{CuO}] + x\mathrm{H_2O}. \quad (10)$$

The cathodic processes pertaining to this potential region are the discharge of anions such as CuO_2^{2-} or $HCuO_2^-$ to either Cu_2O or Cu (see Table 1). It is also interesting to notice that when $E_{\lambda,a}$ extends beyond the potential current peak IV no electroreduction of either CuO_2^{2-} or $HCuO_2^-$ to Cu_2O is observed. This suggests that these species are electrooxidized to CuO.

The charge involved in the potential range of the Cu(II)/Cu(III) couple is smaller than that for current peak I and apparently is independent of the amount of Cu(II) in solution. Following the reaction sequence given above, it seems reasonable to assume that the CuO surface species is one of the reactants [14];

$$\mathrm{CuO} + \mathrm{H_2O} + 2\mathrm{OH^-} \rightleftharpoons \mathrm{Cu(OH)_4^-} + \mathrm{e} \quad (11)$$

although, it might also be possible for the reaction to take place from the $Cu(OH)_2$ species. There is no evidence, however, that a significant proportion of the latter constitutes the surface film at such a high anodic potential.

The Cu(III) species has been proposed earlier [22] and recently identified [21]. The dependence of both the anodic and the cathodic peak heights on $w^{1/2}$ and on $v^{1/2}$ confirms that it entails a soluble species. Nevertheless, the fact that the charge involved is smaller than that corresponding to the CuO species raises the question of why the electrochemical dissolution is so limited. There are no apparent kinetic reasons for this which can be derived from the corresponding E/I trace. In fact, the potential difference between the anodic and the cathodic potential peaks lies close to 0·060 V, as is expected for a reversible diffusion-controlled reaction. Taking into account the fact that the Cu(II)/Cu(III) redox couple is formed in the potential region of the E/I trace corresponding to the O_2 evolution reaction, it is reasonable to suppose that a Cu(III) surface species is also involved as a surface intermediate related to the latter process. This would imply that the outermost surface layer approaches a Cu_2O_3-type structure facilitating the O_2-evolution reaction.

Acknowledgement

This work is part of the research programme of the Electrochemistry Division of INIFTA, sponsored by the Universidad Nacional de La Plata, the Consejo Nacional de Investigaciones Científicas y Técnicas (CONICET), and the Comisión de Investigaciones Científicas de la Provincia de Buenos Aires (CIC). A.M.C.L. thanks the CONICET for the scholarship granted.

References

[1] E. Müller, *Z. Elektrochem.* **13** (1907) 133.
[2] W. Feitknecht and H. W. Linel, *Helv. Chim. Acta* **27** (1944) 775.
[3] A. Hickling and D. Taylor, *Trans. Faraday Soc.* **44** (1948) 262.
[4] L. De Brouckère, F. Bouillon and Y. Bouillon-Nysseu, *Bull. Soc. Chim. Belges* **60** (1951) 26.
[5] S. E. S. El Wakkad and S. H. Emara, *J. Chem. Soc.* (1953) 3508.
[6] J. S. Halliday, *Trans. Faraday Soc.* **50** (1954) 171.
[7] F. Bouillon, J. Piron and J. Esteveres, *Bull. Soc. Chim. Belges* **67** (1958) 643.
[8] A. M. Shams El Din and F. M. Abd El Wahab, *Electrochim. Acta* **9** (1964) 113.

[9] B. Miller, *J. Electrochem. Soc.* **116** (1969) 1675.
[10] H. P. Leckie, *ibid.* **117** (1970) 1478.
[11] M. J. Dignan and D. B. Gibbs, *Canad. J. Chem.* **48** (1970) 1242.
[12] N. A. Hampson, R. J. Latham, J. B. Lee and K. I. MacDonald, *J. Electroanal. Chem.* **31** (1971) 57.
[13] N. A. Hampson, J. B. Lee and K. I. MacDonald *J. Electroanal. Chem.* **32** (1971) 165.
[14] J. Ambrose, R. G. Barradas and D. W. Shoesmith, *ibid.* **47** (1973) 47.
[15] J. Ambrose, R. G. Barradas and D. W. Shoesmith, *ibid.* **47** (1973) 65.
[16] D. D. MacDonald, *J. Electrochem. Soc.* **121** (1974) 651.
[17] D. W. Shoesmith, T. E. Rummery, D. Owen and W. Lee, *ibid.* **123** (1976) 790.
[18] G. Paus, A. J. Calandra and A. J. Arvia, *Ann. Soc. Cient. Arg.* **192** (1971) 35.
[19] G. L. Kehl, 'Fundamentos de la Práctica Metalográfica', Aguilar, Madrid (1963).
[20] W. J. Mc G. Tegart, 'The Electrolytic and Chemical Polishing of Metals in Research and Industry', Pergamon Press, London (1956).
[21] M. Pourbaix, 'Atlas of Electrochemical Equilibria in Aqueous Solutions', Pergamon Press, Oxford (1966).
[22] J. Ambrose, R. G. Barradas and K. Belnike, *J. Electroanal. Chem.* **42** (1973) 146.